Catalysis Communications 187 (2024) 106825

Contents lists available at ScienceDirect

Catalysis Communications

journal homepage: www.elsevier.com/locate/catcom

Ga(*i*Bu)$_3$ supported on *meso* H-ZSM-5: Effect of Si/Al ratio on the activity and selectivity in propane aromatization

Abou Nakad Jessy [a], Daniel Firth [b], Muhammad Taoheed Bisiriyu [a], Kai C. Szeto [a], Nicolas Merle [c], Aimery De Mallmann [a,*], Régis M. Gauvin [d], Laurent Delevoye [c], Unni Olsbye [b,*], Mostafa Taoufik [a,*]

[a] Université Lyon 1, Institut de Chimie Lyon, CPE Lyon, CNRS, UMR 5128 CP2M, 43 Bd du 11 Novembre 1918, F-69616 Villeurbanne Cedex, France
[b] Centre for Materials Science and Nanotechnology (SMN), Department of Chemistry, University of Oslo, N-0371 Oslo, Norway
[c] UCCS (CNRS-UMR 8181), Université Lille Nord de France, USTL, 59652 Villeneuve d'Ascq, France
[d] Chimie ParisTech, PSL University, CNRS, Institut de Recherche de Chimie Paris, 75005 Paris, France

ARTICLE INFO

Keywords:
Bifunctional catalyst
Aromatization/dehydrogenation
SOMC
Ga/*meso* H-ZSM-5 (Si/Al = (25,50,100,200 and ∞)

ABSTRACT

The grafting of Ga(*i*Bu)$_3$ on a series of meso-H-ZSM5, prepared by desilication-dealumination (Si/Al = 25, 50, 100, 200, ∞), has been studied. Materials were characterized by IR, solid-state NMR, BET, ICP and EXAFS. Ga(*i*Bu)$_3$ reacts selectively with silanol groups, yielding a monopodal surface species in the mesopores. Importantly, the Brønsted acidic sites remain intact in the micropores, as revealed by IR and ^{1}H MAS-NMR. These materials can be regarded as bifunctional catalysts, containing isolated Ga sites and Brønsted sites in proximity, suitable for propane aromatization. Catalytic investigations show high activity and selectivity toward aromatics, particularly for low Si/Al ratios.

1. Introduction

Light aromatic compounds such as benzene, toluene and xylene (BTX), are considered essential raw materials for the petrochemical industry and important intermediates toward high value-added chemicals. They are also used as blending mixture to enhance the octane number of gasoline. The increasing demand for BTX has led to a higher interest toward the transformation of light alkanes into aromatics, since light alkanes have become abundant with the discovery of new shale gas reserves [1]. BTX are mainly produced (as by-products) by catalytic reforming or by steam cracking processes [2], however, other methods can be used, from methanol (MTA) [3], syngas (STA) [4] and CO_2 hydrogenation [5]. The "by-product" technologies remain dominant, but are less flexible at aligning with the demand and evolution of the market. Hence, on-purpose technology (where BTX is the main product) is a promising alternative to conventional cracking and reforming processes allowing to secure the market supply. The advantage of on-purpose aromatization is the use of cheap and abundant feedstocks (light alkanes) [2,6]. For example, methane aromatization has been studied, however, due to its low selectivity and the high temperature required during the reaction [7], the use of propane is preferred. On-purpose propane aromatization generally requires a bifunctional catalyst, where the metal sites are responsible for its dehydrogenation into propylene and Brønsted acid sites present in the zeolitic support activate the oligomerization and cyclization of propylene resulting in aromatics [8–11]. Beside the main reaction, coking and cracking may also occur resulting in undesired products. Due to the complexity of this process, many studies were conducted to find a suitable high-performing catalyst. Several metals such as Ga, Pt, Zn and others, have been hosted on zeolites and studied for the aromatization reaction [12–17]. Economically, Ga and Zn are preferred over the expensive noble metal Pt. However, Zn supported on H-ZSM-5 zeolites suffered from high volatility of the active metal under the reaction conditions required (> 500 °C) [6,18,19]. To date, Ga is the most promising metal due to its ability to dehydrogenate and aromatize propane into BTX with a high selectivity and marginal metal leaching [20,21]. Hence, Zeolite (ZSM-5) modified by gallium oxide remains the most used catalyst in industry for propane aromatization as in Cyclar UOP and BP commercialized process [2,22]. The main drawback of propane aromatization on this catalyst is the production of large amounts of light hydrocarbons by cracking side reactions on acidic sites [18], due to the presence of different gallium oxide phases on the surface (particularly clusters or agglomerates). In fact, the catalysts described in the literature are generally obtained via classical synthesis methods such as wetness impregnation (using Ga

* Corresponding authors.
E-mail addresses: Unni.Olsbye@kjemi.uio.no (U. Olsbye), Mostafa.Taoufik@univ-lyon1.fr (M. Taoufik).

https://doi.org/10.1016/j.catcom.2023.106825
Received 19 October 2023; Received in revised form 11 December 2023; Accepted 16 December 2023
Available online 23 December 2023

salts), chemical vapor deposition of $GaCl_3$ (followed by thermal activation or reduction), and even mechanical mixing with Ga_2O_3 [21,23–31]. These uncontrolled synthetic methods are unable to produce the highly disperse and isolated active sites responsible for the aromatization reaction. In fact, Ga-based catalysts prepared by impregnation with high loading of gallium nitrate on the zeolite, leads to the formation of segregated Ga_2O_3 phases on the zeolite surface, responsible for cracking reactions. This method also facilitates the formation of clusters with four gallium centers that have been previously confirmed by EXAFS and ^{71}Ga NMR [32,33]. To overcome these drawbacks and obtain active single sites, an anhydrous route for the incorporation of Ga into the micropores of zeolites, aided by the creation of mesopores in the zeolite, has been proposed. Van Santen et al. described the chemical vapor deposition of trimethylgallium on a H-ZSM-5, with subsequent removal of the methyl groups by treatment with H_2 or O_2 [34,35]. The resulting material yield only propylene via propane dehydrogenation without the formation of any aromatic compounds. This was a result of the total lack of acid sites which are consumed during the preparation of the catalyst, due to the diffusion of the small-sized trimethylgallium through the micropores [34,36,37]. Hence, it is essential to select the precursor with appropriate size. In that context, using a mesoporous H-ZSM-5, we recently developed a bifunctional catalyst through the selective grafting of [Ga(*i*Bu)$_3$] aided by its moderately bulky ligands. Essentially, the Ga precursor is able to successfully attach into the mesopores, while the acidic sites in the micropores remained intact. The resulting bifunctional catalyst exhibited a high propane conversion of 74% with 64 wt% of BTX at 500 °C [38]. The formation of BTX occurs via two steps: dehydrogenation of propane on Ga isolated sites in the mesopores, while the aromatization of the propylene intermediate on the acidic sites takes place in the micropores. Hence, further improvements can eventually be achieved by tuning the acidity of the mesoporous H-ZSM-5 using different Si/Al ratios. It is important to note that a highly active and stable site for propane dehydrogenation is needed to access a high productivity in BTX. We proposed to study the effect of the Brønsted acidity related to Si/Al ratio of *meso* ZSM-5 by using [Ga(*i*Bu)$_3$] as a precursor on the activity and selectivity in propane aromatization.

The aim of the present work was to prepare a bifunctional Ga catalyst by immobilizing [Ga(*i*Bu)$_3$] on meso H-ZSM-5-$_{250}$ (Si/Al = 25, 50, 100, 200 and ∞). The resulting materials were evaluated in propane aromatization in order to select the most promising support. The catalysts were characterized by DRIFT, solid-state NMR, BET, XAFS and mass balance analysis.

2. Experimental section

2.1. General procedures

All experiments were carried out under a controlled atmosphere, using Schlenk and glovebox techniques for organometallic synthesis. For the synthesis and treatment of supported species, reactions were carried out using high-vacuum lines (ca. 1 mPa) and gloveboxes. Pentane was distilled from NaK and degassed using freeze-pump-thaw cycles. [Ga(*i*Bu)$_3$] was synthesized according to a published method [39].

2.2. Preparation of Meso H-ZSM-5-$_{250}$

Mesoporous ZSM-5 samples were prepared in three steps from microporous ZSM-5 (micro-ZSM-5). The first step consisted in the syntheses of Micro-ZSM-5 with different Si/Al ratios following procedures previously reported by Jacobs and Martens [40] combining silica with NaOH and water (Solution 1), a premixed solution of tetrapropylammonium bromide and water (Solution 2) followed by the addition of a premixed solution of sodium aluminate and water (Solution 3) to achieve the desired Si/Al gel ratio (Table A1). The second step was dedicated to the desilication-dealumination [41] of the calcined microporous ZSM-5 samples to obtain *meso*pores. The final step consisted in an ion exchange to get the acidic form of meso-ZSM-5 (Si/Al = 25, 50, 100, 200 and ∞) followed by a calcination at 550 °C under air and a dehydroxylation at 250 °C [38].

2.3. Preparation and characterization of Ga(*i*Bu)$_3$/meso H-ZSM-5-$_{250}$

A mixture of [Ga(*i*Bu)$_3$] (200 mg, 0.80 mmol) and meso-H-ZSM-5-$_{250}$ (25, 50, 100, 200 and ∞) (1 g) in pentane (10 mL) was stirred at 25 °C for 4 h. After filtration, the solid was washed 4 times with pentane and the washing fractions were transferred to another reactor in order to quantify the amount of isobutane evolved during grafting. The resulting colorless powder was dried under vacuum (1 mPa) at 70 °C.

2.4. Analytical and spectroscopic procedures

Elemental analyses were carried out at Mikroanalytisches Labor Pascher, Remagen (Germany). Gas-phase analyses were performed on a Hewlett-Packard 5890 series II gas chromatograph, equipped with a flame ionization detector and HP PLOT KCl/Al_2O_3 column (50 m × 0.32 mm). Diffuse reflectance IR spectra were collected in an airtight IR cell equipped with CaF_2 window, using a Nicolet 6700 FT-IR spectrophotometer recording 64 scans at 4 cm^{-1} resolutions. Nitrogen adsorption/desorption experiments were performed in Micrometrics ASAP 2020 instrument. X-ray diffraction patterns were recorded in a Bruker D8 diffractometer in Bragg-Bretano geometry, using monochromatic Cu Kα1 radiation.

Solid-state NMR spectra were acquired on Bruker Avance 500 and Bruker Avance III 800 spectrometers (respectively 11.7 and 18.8 T). For ^{1}H experiments, the spinning frequency was 20 kHz, the recycle delay was 30 s for meso-H-ZSM-5$_{250}$ (25, 50, 100, 200 and ∞) and 10 s for Ga(*i*Bu)$_3$/meso-H-ZSM-5$_{250}$ (25, 50, 100, 200 and ∞), and 16 scans were collected using a 90° pulse excitation of 2.25 μs. The ^{13}C CP-MAS NMR spectrum was obtained at 11.7 T using the CP-MAS pulse sequence and a high-power ^{1}H decoupling at an RF field amplitude of 70 kHz. The spinning frequency was set to 10 kHz.

EXAFS spectra were recorded at ESRF, using BM23 beam-line, at room temperature at the gallium K-edge (10.37 keV). A pair of Si(111) crystals was used as monochromator and a system based on a total reflection through a double X-ray mirror with an incidence angle variable from 2 to 5 mrad allowed harmonic rejection close to 10^{-5} level [42]. The spectra were recorded in the transmission mode between 10.1 and 11.4 keV. Four scans were collected for each sample. Each data set was collected simultaneously with a W metal foil (L_{III} edge at 10.207 keV) and was later aligned according to that reference. The Ga supported samples were packaged within an argon filled glovebox in a double air-tight sample holder equipped with kapton windows. The data analyses were carried out using the program "Athena" [43] and the EXAFS fitting program "RoundMidnight", from the "MAX" package [44], using spherical waves. The program FEFF8 was used to calculate theoretical files for the total central atom loss factor, r_c, the electron mean free path, λ, the phases, ϕ_i, ϕ_c and amplitudes, F_i, based on model clusters of atoms [45]. The refinements were carried out by fitting the structural parameters N_i, R_i, σ_i and the energy shift, ΔE_0 (the same for all shells of a same structure was used):

$$\chi(k) \cong S_0^2 * r_c(k) * \sum_{i=1}^{n} \frac{N_i F_i(k, R_i)}{kR_i^2} * exp\left(\frac{-2R_i}{\lambda(k)}\right) * exp\left(-2\sigma_i^2 k^2\right) * sin[2kR_i + \Phi_i(k, R_i) + \Phi_c(k)]$$

3. Results and discussion

3.1. Preparation and characterization of meso-H-ZSM-5$_{-250}$ with Si/Al ratio 25, 50, 100, 200 and ∞

Zeolites are well-defined crystalline, thermally stable,

aluminosilicate materials with regular pores and channels, and a high specific surface area, ranging typically from 300 to 700 m^2/g [46]. These materials are widely used in the industry as heterogeneous catalysts for a wide range of processes, due to their strong acidity and uniform micropores (< 2 nm in diameter) [47,48]. However, their catalytic activity suffers from diffusional limitations in the presence of bulky reactant or products, resulting in pore blocking [49–51]. The creation of mesopores connected to the zeolite micropores is a promising solution to minimize and overcome the diffusion limitation [10,52,53]. In this way, the micropores of the zeolite are effectively shortened while the formation of mesopores increases the external surface area of the zeolite, allowing the accessibility of the reactants to a larger number of pores. Several synthesis routes have been reported in the literature, such as post-treatment and template assembly for the preparation of hierarchically porous zeolites [54]. In order to establish the correlation between the acidity of the zeolites with the catalytic activity in propane aromatization in presence or absence of Ga, we synthesized a series of *meso*-zeolites (meso H-ZSM-5) with different Si/Al ratios: 25, 50, 100, 200 and ∞) using the procedures described in the experimental section including the preparation method of micro-zeolites described by Jacobs and Martens [40]. The zeolites (H-ZSM-5 and meso H-ZSM-5) have been characterized before and after post-synthesis by XRD, SEM, EDX and BET. The meso-zeolites with different Si/Al obtained after calcination and dehydroxylation at 250 °C were characterized by DRIFT, solid state NMR and BET before the grafting of gallium organometallic complex.

The change in crystalline structure of ZSM-5 before and after NaOH treatment was evaluated using powder X-ray diffraction (PXRD patterns) technique (Fig. A1). The corresponding peaks for crystalline ZSM-5 are observed in both cases confirming the expected MFI framework. However, a slight difference between phases was observed when the Si/Al ratio increased and after post-treatment with NaOH. Similar results were also reported by Xue et al. [55]. In addition to XRD, SEM images of the H-ZSM-5 crystals confirmed the formation of the expected coffin-like crystals typically seen for ZSM-5. SEM images also showed that typical crystal sizes are within the required range of 1–5 μm (Fig. A2). It was noted that with increasing the aluminum content of the synthesized gel (Si/Al ratio lower than 50), a slight change in the morphology of the H-ZSM-5 was observed, the crystals becoming less well defined and more polycrystalline in nature. The morphology of the crystals remained unchanged following the NaOH treatment of the microporous H-ZSM-5 to form the *meso*porous supports (meso H-ZSM-5, Si/Al = 25, 50, 100, 200, ∞) (Fig. A3).

Moreover, EDX analysis of these samples confirmed that the Si/Al content of the synthesized H-ZSM-5 remained practically unchanged for *meso* H-ZSM-5 after the NaOH treatment (Table A2). To gain more information about the porous properties of the mesoporous ZSM-5, we performed N_2 physisorption measurements. Figs. A4-A8 show the N_2 adsorption/desorption isotherms of H-ZSM-5 and meso H-ZSM-5 with the different Si/Al ratio. In figs. A4a-A8a, H-ZSM-5 adsorption/desorption behavior is attributed to a type I isotherm, typical of a microporous zeolite, with the adsorption being slightly higher for those samples with higher Si/Al ratios. In comparison with figs. A4b-A8b, the post-treatment of these samples with NaOH solution resulting in *meso* H-ZSM-5 exhibited a type IV behavior and greater adsorption capacity associated with the production of mesopores. It should be noted that as the Si/Al ratio of the parent ZSM-5 samples increased, treated samples (*meso* H-ZSM-5) were less mesoporous in character and showed decreased adsorption capacity (Table A2). This is likely due to the increasing crystallinity (with increasing Si content) of the samples making the crystals less susceptible to the desilication-dealumination process [41]. The pore volumes and surface areas of the meso H-ZSM-5 samples were also evaluated using N_2 physisorption measurements (Table A2). The post treatment with NaOH of H-ZSM-5 led to an increase in the total pore volumes and specifically in the mesopores volume. A slight increase in the BET surface area was observed (for Si/Al = 25 and 50), as calculated by BJH method. The above results confirmed that *meso*pore formation in the synthesized ZSM-5 samples depends on Si/Al ratios.

In order to control the grafting reaction of Ga precursor on the mesoporous zeolites, meso-H-ZSM-5 with different ratio (Si/Al = 25, 50, 100, 200 and ∞) were then subjected to dehydroxylation at 250 °C under high vacuum (1 mPa), affording meso H-ZSM-5-$_{250}$. The resulting materials were characterized by N_2 adsorption/desorption, DRIFT and ^{1}H MAS NMR and were tested in propane aromatization, without dehydrogenation Ga active site. A high specific surface area, between 350 and 400 m^2/g, was obtained with large total pores volume in the range of 0.21 to 0.27 cm^3/g (Table A3). For example, Fig. 1 displays the N_2 adsorption/desorption feature of *meso* H-ZSM-5-$_{250}$ with Si/Al = 50, revealing a BET surface of 381.6 m^2/g with large pore volumes of 0.27 cm^3/g. These results confirm that at 250 °C the zeolite properties (large BET surface and pore volumes) are conserved. The highest total pores volume and *meso*pores volume were obtained for meso-zeolites with the lowest Si/Al ratios (Si/Al = 25 and 50) and decreases with the increase of silicon proportion in the support (Table A3).

The presence of both isolated silanols (≡SiOH) and Brønsted acid sites (≡Si(*OH*)Al) was reflected by characteristic bands in the DRIFT spectrum of *meso* H-ZSM-5-$_{250}$ (Si/Al = 50) at 3743 and 3608 cm^{-1}, respectively (Left in Fig. 2). The other weak and unresolved band centered at 3663 cm^{-1} corresponded to AlOH species associated with extra-framework alumina (EFA), generated during desilication-dealumination. For the comparison of all the meso H-ZSM-5-$_{250}$ with different ratios, we observed that the vibration band at 3740 cm^{-1} characteristic of isolated silanols and the band at 3608 cm^{-1} attributed to the acidity decreased with increasing Si/Al (Fig. 2). Consequently, the acidity of the support decreases when Si/Al ratio rises [41,56]. However, the broad band centered at 3450 cm^{-1} attributed to vicinal silanols increased when Si/Al ratio increased, in particular for Si/Al = 200 and ∞. These vicinal silanols were already observed in the case of SiO_2 dehydroxylated at low temperatures (200 °C) and have been reported to be unreactive with organometallic complexes [57,58]. Additionally, no band at 3608 cm^{-1} attributed to Brønsted acidic protons was observed in the spectrum of *meso* H-ZSM-250 (Si/Al = ∞). Thus, the employed post treatment method of MFI materials with different Si/Al ratio resulted in meso-pore creation and simultaneously generated additional silanol groups suitable for grafting of the organometallic precursor (vide infra). Since the crystallinity (Fig. A1) and morphology (Fig. A2) were different as the Si/Al ratio increases, the desilication-dealumination process appeared to be less susceptible, and thereby resulted in less defect/silanol formation (for higher Si/Al ratio), also supported by DRIFT (Fig. 2).

Accordingly, the characterization of these materials using high field solid-state NMR spectroscopy confirmed the previous result. The spectra obtained after dehydroxylation of *meso* H-ZSM-5 with different ratios in Fig. 2 were in agreement with reported literature, in which three main signals were distinguished [59–62]. The aromatization activity is generally reported to be catalyzed by the Brønsted acid site (BAS), that shows a signal at around 4 ppm in ^{1}H MAS NMR (Fig. 2, right). The intensity of this peak decreased as the Si/Al ratio increased from 25 to 50, attributed to the decreasing incorporation of Al into the framework and concomitant charge balance by the Brønsted proton. For example, the ^{1}H NMR spectra of *meso*-H-ZSM-5-$_{250}$ (Si/Al = 25 and 50) showed three major signals at 3.9, 2.5, and 1.6 ppm (right in Fig. 2, black and red lines). These are attributed to Brønsted acidic protons (≡Si(*OH*)Al-type) [63], extra-framework alumina (EFA) hydroxyls [64], and non-interacting silanol protons [63], respectively. In fact, the peak obtained at 3.9 ppm corresponds to a range of bridging hydroxyl groups attached to more than one aluminum ion and likely also to those between Si and Al atoms. Whereas, in the case of *meso* H-ZSM-5-$_{250}$ (Si/Al = 100 and 200), the same signals were obtained but with a shift of the peak from 3.9 to 4.7 ppm (right in Fig. 2), which was assigned in the literature to another type of acid site, where the hydroxyl groups were attached to more than one Al ion [65,66]. The ^{1}H NMR spectrum of *meso*

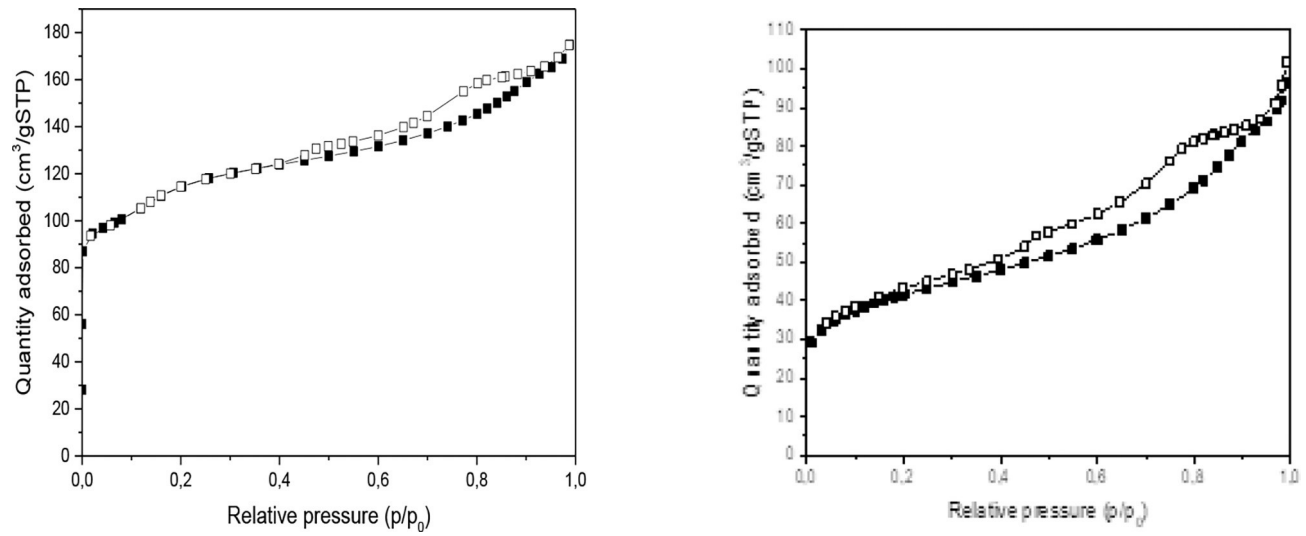

Fig. 1. Left: N_2 adsorption (closed symbols) /desorption (open symbols) isotherms for meso-H-ZSM-5-$_{250}$ (Si/Al =50). Right: N_2 adsorption (closed symbols) /desorption (open symbols) isotherms for Ga(^{i}Bu)$_3$/meso-H-ZSM-5-$_{250}$ (Si/Al =50).

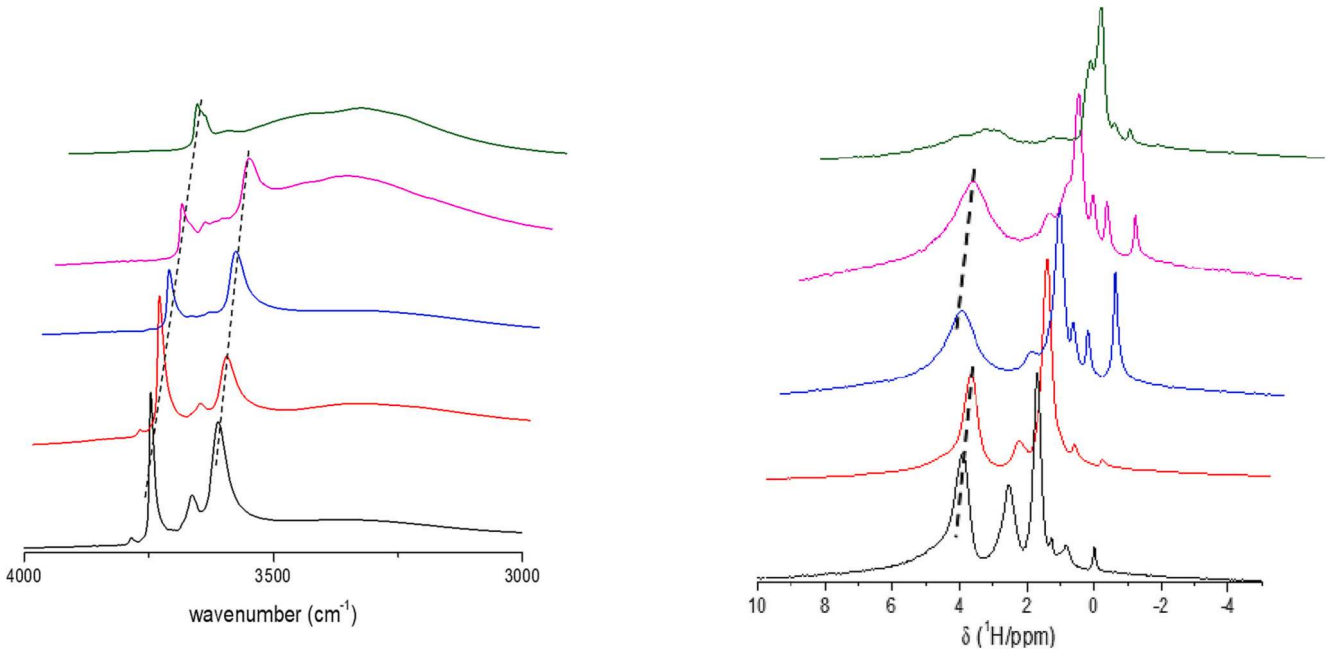

Fig. 2. Left: DRIFT and Right: ^{1}H NMR spectra of meso H-ZSM-5-$_{250}$: Si/Al = 25 (black), Si/Al = 50 (red), Si/Al = 100 (blue), Si/Al = 200 (magenta), Si/Al = ∞ (olive) (18.8 T, 20 kHz, d_1 = 20 s). (For interpretation of the references to colour in this figure legend, the reader is referred to the web version of this article.)

H-ZSM-5-$_{250}$ (Si/Al = ∞) featured two intense signals, namely a sharp, asymmetric contribution at 1.6 ppm for non-interacting silanols, accompanied with a peak at 2 ppm probably due to the presence of H-bonded vicinal silanol (right in Fig. 2). These results confirmed that the *meso*-zeolites with ratio of Si/Al from 25 to 200 show Brønsted acidity compared to non-acidic meso H-ZSM-5-$_{250}$ (Si/Al = ∞). This is in agreement with the work reported by Shirazi et al. who demonstrated by using NH_3-TPD profile that the total acidity of the *meso*-zeolites decreases when Si/Al ratio increases [56].

3.2. Catalytic properties of meso H-ZSM-5-$_{250}$ (Si/Al = 25, 50, 100, 200 and ∞) in propane aromatization

In order to evaluate the catalytic activity of the zeolites as a function of their acidity, related to their Si/Al ratio, *meso* H-ZSM-5-$_{250}$ (Si/Al = 25, 50, 100, 200 and ∞) supports were exposed to propane in a continuous flow reactor at $T = 580$ °C, $P = 1$ bar and with a total flow of 10 mL.min^{-1} (5% C_3 in Ar). The propane conversion obtained on the bare meso-zeolites with several Si/Al ratios as well as the average selectivity for light hydrocarbons and aromatics are depicted in Fig. A9. Both meso H-ZSM-5-$_{250}$ with the lowest Si/Al ratios, 25 and 50 exhibited an important C_3 conversion, 87 and 67%, respectively. The average selectivity in aromatics for meso H-ZSM-5-$_{250}$ (Si/Al = 25 and 50) was significant: 45 and 31 wt%, along with 55 and 69 wt% of light hydrocarbons, respectively. The formation of large amounts of aromatics confirmed that these supports were highly acidic and capable of converting propene intermediate into the targeted products, and hence justify the low amount of propene observed in the gas phase during the catalytic test (3.1 and 8 wt% for Si/Al = 25 and 50, respectively). The lighter compounds were produced from acidic cracking, reported to be

catalyzed by a penta-coordinated carbonium ion [67]. For Si/Al = 100 and 200, the C_3 conversion (38 and 28%, respectively) and the selectivity toward aromatics (9 and 7 wt%) were lower compared to the previously described zeolites with lower Si/Al ratios. This may be attributed to the low amount and the different nature of the zeolite Brønsted acid sites. It is important to note that the relative selectivity toward propene was higher compared to the previous zeolites, with 16.3 and 22.3 wt% for *meso* H-ZSM-5-$_{250}$ (Si/Al = 100 and 200), respectively. The role of the acid sites in producing aromatics was confirmed when meso H-ZSM-5-$_{250}$ with no Brønsted site (Si/Al = ∞) was studied for propane aromatization and produced only light hydrocarbons with propene as a major component (59.1 wt%) for 2% conversion of propane. All these results revealed that the meso H-ZSM-5-$_{250}$ with low Si/Al ratios (25 and 50) were more acidic and more selective for aromatics than the other *meso* H-ZSM-5-$_{250}$ with Si/Al higher ratios (Fig. A9, Right).

3.3. Preparation and characterization of [Ga(iBu)$_3$] supported on meso H-ZSM-5-$_{250}$

The grafting reaction of meso H-ZSM-5-$_{250}$ with different Si/Al ratios was carried out with an excess of [Ga(*i*Bu)$_3$] in pentane at room temperature. The resulting materials were extensively washed with pentane. The washing fractions and the gas evolved were transferred to another reactor in order to measure by GC the amount of isobutane released during the grafting reaction. The white powders were dried under vacuum (1 mPa) at room temperature for 3 h, affording Ga(*i*Bu)$_3$/*meso* H-ZSM-5-$_{250}$ (Si/Al = 25) (A), Ga(*i*Bu)$_3$/meso H-ZSM-5-$_{250}$ (Si/Al = 50) (B), Ga(*i*Bu)$_3$/meso H-ZSM-5-$_{250}$ (Si/Al = 100) (C), Ga(*i*Bu)$_3$/meso H-ZSM-5-$_{250}$ (Si/Al = 200) (D) and Ga(*i*Bu)$_3$/meso H-ZSM-5-$_{250}$ (Si/Al = ∞) (E) materials. These materials were characterized by DRIFT, solid-state NMR, EXAFS, BET and mass balance analysis.

The gallium modified samples were characterized by IR spectroscopy. In particular, the DRIFT spectrum of the material Ga(*i*Bu)$_3$/meso H-ZSM-5-$_{250}$ (Si/Al = 50) (B) revealed significant consumption of isolated silanols, supported by the attenuation of the intensity of the band at 3743 cm^{-1} (Fig. 3b). The bands appearing at 2800–3000 cm^{-1} are attributed to ν(C—H) vibrations of alkyl moieties. The large and intense band centered at 3475 cm^{-1} is due to Brønsted acidic protons in interaction with pentane causing a red shift, from 3601 cm^{-1} [68]. Upon thermal treatment of the sample at 70 °C under high vacuum for 12 h, the band at 3601 cm^{-1} reappears confirming the resistance of such sites during the grafting. This result further demonstrated that the grafting occurred selectively on the silanol groups located in the mesopores, while the Brønsted acidic sites in the micropores were not affected due to the high kinetic diameter of the gallium precursor that does not allow any access to the micropores contrarily to Ga(Me)$_3$, used by van Santen et al. [34,35]. Similar behaviors were also observed in the case of catalysts (A), (C), (D) and (E) (Fig. A10-A13, respectively). Contrarily to the case of (A) and (B), a partial consumption of isolated silanol groups was observed from the IR spectra of (C), (D) and (E) (decrease of 3743 cm^{-1} band intensity).

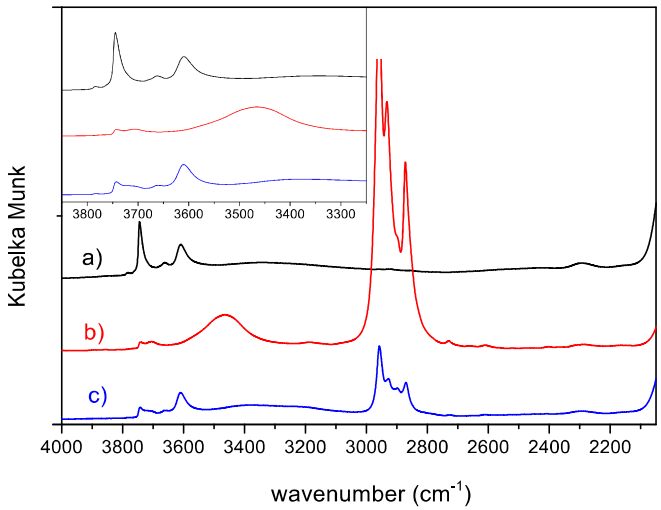

Fig. 3. DRIFT spectra a) of meso H-ZSM-5-$_{250}$ (Si/Al = 50), b) after reaction with [Ga(^{i}Bu)$_3$] in pentane at 25 °C and (c) after thermal treatment at 70 °C and high vacuum for 12 h.

According to elemental analysis, the capability to graft gallium at room temperature varies on the different supports and strongly depends on the Si/Al ratio. When the latter increased from 25 to infinite, the grafted amount of Ga decreased from 1 to 0.08 wt% (Table 1). This is in accordance with the decrease in the volume of the *meso*pores when the Si/Al ratio increases, as shown in Table A3. The low Ga loading obtained on *meso* H-ZSM-5-$_{250}$ (Si/Al = 100, 200 and ∞) can be explained by the blockage of the mesopores by the organometallic complex at the beginning of the grafting reaction, thus limiting the diffusion of the complex into the *meso*pores. These results are in agreement with the DRIFT spectra of (C), (D) and (E) that showed only a partial consumption of silanols (Figs. A11-A13).

The quantification by GC analysis of the gas evolved during the grafting reaction displayed a release of 0.9 isobutane in the case of [Ga(*i*Bu)$_3$] on *meso* H-ZSM-5-$_{250}$ (Si/Al = 50) (B). Additionally, elemental analysis of (B), contains 0.92 wt% of Ga and 1.7 wt% of C. These results suggested that the surface gallium species was predominantly monopodal, bearing two isobutyl fragments, as reported in the case of [Ga(*i*Bu)$_3$] on *meso* H-ZSM-5-$_{250}$ (Si/Al = 20) [38]. The same features were obtained for the other materials (Scheme 1), independently of the Si/Al ratio (see Table 2), suggesting that the same surface species were formed.

Additional information concerning the gallium modified meso H-ZSM-5-$_{250}$ were obtained via N_2 physisorption measurements. Catalysts (A) and (B) obtained on meso H-ZSM-5-$_{250}$ with low Si/Al ratio (25 and 50) revealed an important decrease of their surface area as well as of their total pore volume (Table A4 and right in Fig. 1). This decrease was previously observed while grafting $GaMe_3$ on H-ZSM-5 and was attributed to the pore blockage [34]. Consequently, it is expected that [Ga(*i*Bu)$_3$] was grafted mainly in the *meso*pores and is unable to access the 10-membered ring system of the ZSM-5 bearing the Brønsted acid sites (in micropores) as revealed by DRIFT. For the rest of the supports (Si/Al = 100, 200 and ∞), a slight decrease in the surface area and in the total volume pores was observed which is in agreement with the partial grafting of [Ga(*i*Bu)$_3$] in the mesopores as revealed by elemental analysis and DRIFT spectra.

Complementary evidence of the grafting was obtained by using solid-state MAS NMR. In the ^{1}H MAS NMR spectrum of Ga(*i*Bu)$_3$/*meso* H-ZSM-5-$_{250}$ (Si/Al = 50) (Fig. 4, left), several signals appeared at 0.9, 2 and 4 ppm corresponding to methyl groups of isobutyl fragments, to the Al-OH (EFA) and to the Brønsted acid sites, respectively. The weak peak above 7 ppm has previously been assigned to disturbed BAS, most likely due to the presence of pentane traces which is difficult to completely remove. The ^{13}C CP MAS spectrum consisted in two signals at 25.6 and 30.9 ppm, attributed to *C*H$_3$ and *C*H from the isobutyl groups, respectively. Methylene carbon Ga-*C*H$_2$, expected to resonate around 27 ppm according to published works is hidden by the large peaks (Fig. 4, right).

Table 1
Mass balance analysis of catalysts (A), (B), (C), (D) and (E).

Samples	%$_{wt}$Ga	%$_{wt}$C	*i*-BuH/Ga
Ga(*i*Bu)$_3$/meso H-ZSM-5-$_{250}$ (Si/Al = 25) (A)	1	1.75	0.9
Ga(*i*Bu)$_3$/meso H-ZSM-5-$_{250}$ (Si/Al = 50) (B)	0.92	1.7	0.89
Ga(*i*Bu)$_3$/meso H-ZSM-5-$_{250}$ (Si/Al = 100) (C)	0.25	0.45	0.85
Ga(*i*Bu)$_3$/meso H-ZSM-5-$_{250}$ (Si/Al = 200) (D)	0.11	0.2	0.87
Ga(*i*Bu)$_3$/meso H-ZSM-5-$_{250}$ (Si/Al = ∞) (E)	0.08	n.d	0.82

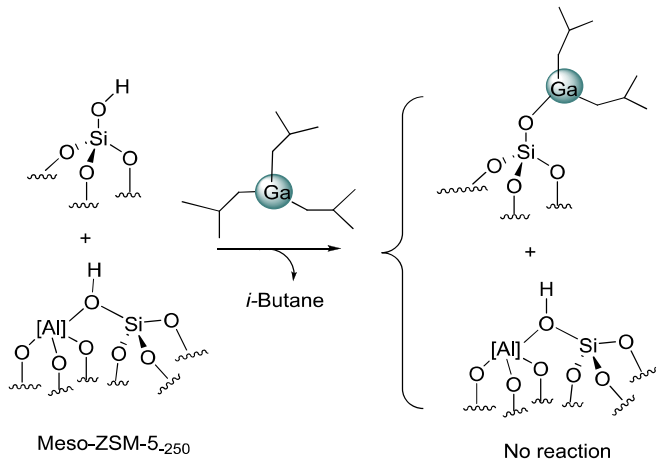

Scheme 1. Grafting of [Ga(*i*Bu)$_3$] onto meso H-ZSM-5$_{-250}$ (Si/Al = 25, 50, 100, 200 and ∞)

Table 2
Parameters obtained from the fit of the EXAFS spectrum for Ga(*i*Bu)$_3$/H-ZSM-5-$_{250}$ (Si/Al = 50).[a] The error interval generated by the fitting program "RoundMidnight" is indicated for each variable parameter between parentheses.

Path[a]	*N*[b]	*R* (Å)	σ^2 (Å^2)
Ga-O	1	1.807(12)	0.0042(16)
Ga–C1	2	1.98(2)	0.0025(10)
Ga–O<	1	2.47(4)	0.017(8)
Ga–C2	2	3.00(2)	0.0036(18)
Ga–Si	1	3.25(7)	0.057(75)

[a] Δk: [2.0–13.4 Å^{-1}] - ΔR: [0.4–3.9 Å]; $S_0^2 = 0.96$; ΔE0 = 7.0 ± 0.7 eV (the same for all shells); Fit residue: ρ = 3.4%; Quality factor: $(\Delta\chi)^2/\nu = 2.57$ ($\nu = 15/26$).

Similar behavior was observed in the NMR spectra of catalysts (A), (C), (D) and (E) (Figs. A14-A17).

To conclude, DRIFT, solid-state NMR and mass balance analysis are in agreement with the formation of a monopodal species on the different *meso* H-ZSM-5-$_{250}$ (Scheme 1).

The local structure of the material Ga(*i*Bu)$_3$/meso H-ZSM-5-$_{250}$ (Si/Al = 50) was investigated by X-ray absorption spectroscopy at the Ga K-edge. The EXAFS spectrum with the corresponding Fourier-transformed magnitude and imaginary component for [Ga(*i*Bu)$_3$] grafted onto meso-H-ZSM-5-$_{250}$ (Si/Al = 50) are shown in Fig. 5 and the fit parameters given in Table 2. In this spectrum, we observed two principal maxima. A peak between 0.8 and 2.0 Å, corresponds to scattering from light atoms (O, C) in the first coordination sphere of Ga. In fact, Ga is bonded to 2C atoms of the isobutyl ligands, as well as 1 O atom derived from the support, in agreement with the mass balance analysis (vide supra), in which monopodal species were proposed (Table 2 and Scheme 1). The fitted Ga—O (1.807(12) Å) and Ga—C (1.98(2) Å) bond distances are both slightly shorter than values previously reported by our laboratory for grafted [Ga(*i*Bu)$_3$] on meso H-ZSM-5-$_{250}$ (Si/Al = 20), 1.88(1) and 2.07(2) Å, respectively [38]. However, the range of Ga—C distances reported for terminal Ga—C bonds in [HGa(*i*Pr)$_2$]$_3$, 1.995–2.131 Å, is compatible with what we observed in the case of catalyst (B) [69]. Moreover, the Ga—O distance (1.807 Å) falls in the range expected for terminal Ga-OR bond lengths (1.79–1.89 Å) [70,71].

The other maxima in the FT magnitude between 2.2 and 3.0 Å is assigned to non-bonded atoms in the second coordination sphere of the Ga. The curve fit is compatible with the presence of two non-bonded C atoms at a distance of 3.00 Å, as Ga is surrounded by two isobutyl ligands, each bearing a secondary carbon. In addition, two other long paths: Ga-O (2.47 Å) and Ga—Si (3.25 Å), make it possible to obtain a good fit of the experimental spectrum. In summary, all the above contributions from EXAFS are consistent with the presence of grafted monopodal species, [(≡SiO)Ga(*i*Bu)$_2$].

3.4. Catalytic activity of [Ga(iBu)$_3$] catalysts on meso H-ZSM-5-$_{250}$

In order to evaluate the effect of the Si/Al ratio in propane aromatization, the resulting grafted materials were tested in the same conditions as the bare zeolitic support meso H-ZSM-5-$_{250}$. Ga(*i*Bu)$_3$/meso H-ZSM-5-$_{250}$ (Si/Al = 50) displayed a higher conversion (88% vs 67%) than the non-modified meso-zeolite (Si/Al = 50) at early times on stream (Fig. A18). At 900 min, the products consisted in 36.6 wt% of benzene, 26.1 wt% of toluene, 13 wt% of methane, 10.5 wt% of ethene, 7 wt% of ethane and 5.7 wt% of propene, along with traces of C4. It is important to note that the selectivity toward aromatics remains constant over the time on stream. The low amount of propene indicates the capacity of this catalyst, more specifically of the Brønsted acid sites located in the micropores of the zeolite, to catalyze oligomerization and aromatization of the olefins intermediates [24]. Moreover, the presence of Ga in the zeolite resulted in an increased selectivity toward aromatics (up to 64 wt% along with 36 wt% of light hydrocarbons). Fig. A18 highlights the importance of Ga in the mesopores of the zeolite (Si/Al = 50). The presence of Ga led to a considerable difference in the product distribution. The essential features were reduction of the cracking products observed earlier in the bare zeolite and promotion of aromatization reactions. The average selectivity of aromatics doubled (64 wt %) when gallium was grafted on the meso-zeolite (Si/Al = 50) compared to 32 wt% of aromatics for the bare support. It is evident that gallium has a substantial effect for this reaction. As the well accepted mechanism for propane aromatization involves propane dehydrogenation accompanied by propene oligomerization/cyclization, the initial dehydrogenation step is thus important and will govern the activity and selectivity. Supported single site gallium is known to be a promising alkane dehydrogenation phase and converts part of the propane to propene. The

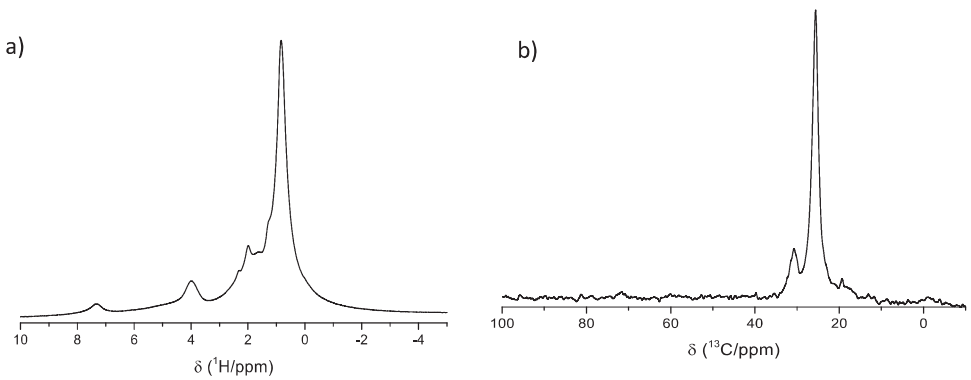

Fig. 4. a) ^{1}H MAS and b) ^{13}C CP MAS NMR spectra of of Ga(^{i}Bu)$_3$/meso H-ZSM-5-$_{250}$ (Si/Al = 50), (B) (11.7 T, 10 kHz).

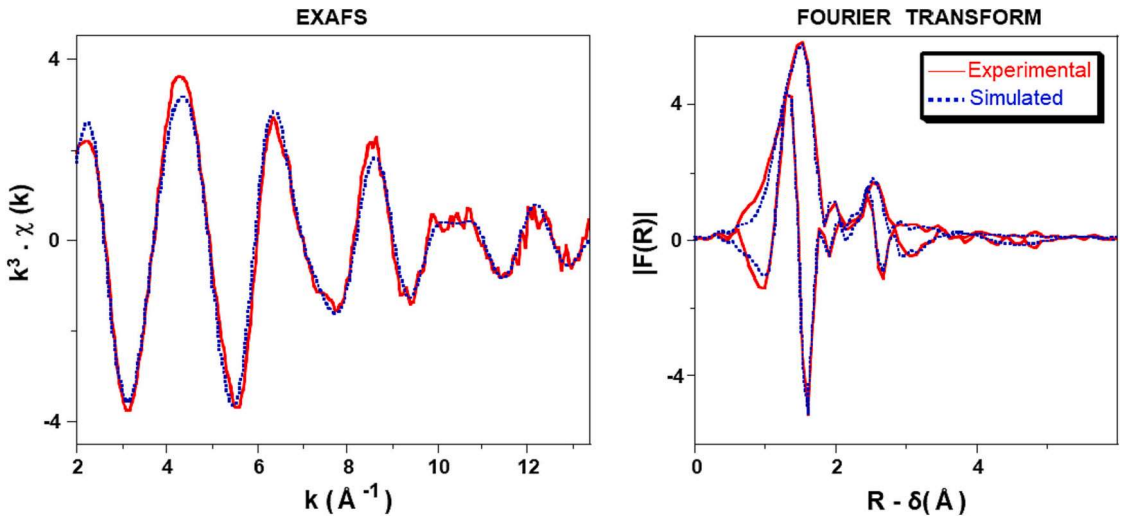

Fig. 5. Ga K-edge k^3-weighted EXAFS (left) and Fourier transform (right, modulus and imaginary part; distances uncorrected from phase shifts) of Ga(^{i}Bu)$_3$/H-ZSM-5-$_{250}$ (Si/Al = 50). Solid lines: Experimental; Dashed lines: Fit (spherical wave theory).

generated propene can readily react with Brønsted acidic sites located in the micropores to undergo oligomerization/cyclization. Such combination is essential in order to achieve high activity and selectivity in BTX. On the other hand, in the absence of gallium, mainly cracking reactions of propane over Brønsted acidic sites are observed.

The catalytic performance of all the catalysts is summarized in Fig. 6. Catalyst (A) revealed also a high conversion of 97% with an important selectivity toward aromatics of 66 wt% along with 34 wt% of light hydrocarbons (Fig. A19). The lowest amount of propene was observed with the most acidic catalysts (A) and (B) with lowest ratios of Si/Al (25 and 50), exhibiting only 2.2 and 5.3 wt% (Fig. 6b). Catalysts (C) and (D) with higher ratios of Si/Al (100 and 200) showed a quick deactivation and a lower amount of BTX compounds produced (Fig. 7), due to the low acidity of the used supports. Consequently, the amount of propene produced in these catalysts increased (10 wt% for (C) and 16.2 wt% for (D)), compared to catalysts (A) and (B) (Figs. A21–22). The deactivation was more pronounced with the increase of silica amount in the support. Hence, Ga(*i*Bu)$_3$/*meso* H-ZSM-5-$_{250}$ (Si/Al = ∞) revealed a very low conversion of 2.5% with high selectivity in the dehydrogenation product, propene (71.8 wt%) and absence of BTX (Fig. A23). This result can be explained by the absence of Brønsted acid sites in this support as shown by DRIFT and ^{1}H MAS NMR. In conclusion, the selectivity in aromatics is related to the Si/Al ratio of the [Ga(*i*Bu)$_3$] on meso H-ZSM-5-$_{250}$, that decreases when Si/Al ratio increases. This tendency was also reported earlier for GaO_x supported on microporous H-ZSM-5 prepared by incipient wetness impregnation [27]. The enhanced activity [72] observed in this case can be attributed to the control immobilization of isolated Ga site through the meso-porous zeolite support. It is widely accepted that propane aromatization proceeds consecutively via propane dehydrogenation followed by propene cyclization/aromatization where the immobilized Ga is responsible for the rate determining propane dehydrogenation step. Recent studies have revealed that isolated Ga is the active species in alkane dehydrogenation [73] which exhibits higher activity than Ga_2O_3. Having isolated Ga highly dispersed in the zeolite support will offer a beneficial effect on the cascade reaction.

On *meso* H-ZSM-5-$_{250}$ (Si/Al = 50), we observed a high selectivity in aromatics accompanied with the formation of light hydrocarbons. These findings showed that several reactions like cracking, dehydrogenation, aromatization and hydrogenolysis occurred simultaneously during propane aromatization. These reactions are expected to be somewhat tunable by thermodynamic parameters such as the reaction temperature. Choudhary et al. demonstrated that the selectivity and distribution of the aromatic products were highly affected by the operating temperature [74,75]. Therefore, supplementary efforts were made to investigate the influence of temperature and propane concentration with respect to the product selectivity and distribution of aromatics during propane aromatization over Ga(*i*Bu)$_3$/*meso* H-ZSM-5-$_{250}$ (Si/Al = 50). Based on the data obtained at 580 °C, we studied the propane aromatization on catalyst (B) at 500 and 540 °C in the same conditions (total flow of 10 mL.min^{-1} (5% of C_3 in Ar)). Decreasing the temperature

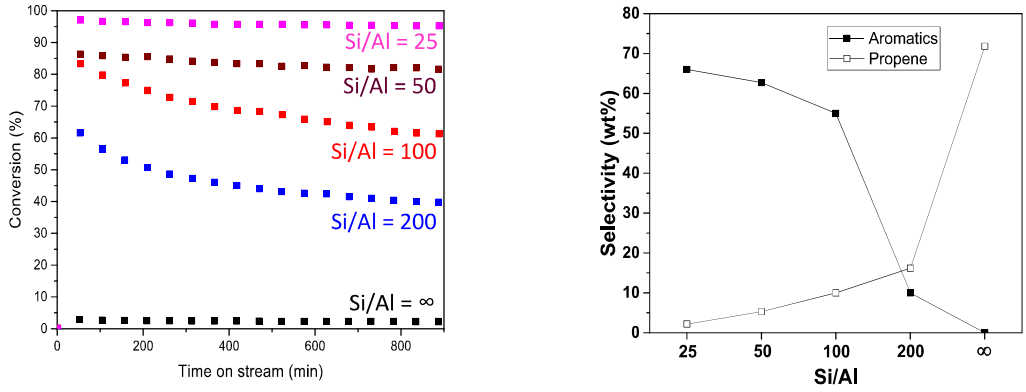

Fig. 6. Left: propane conversion of [Ga(^{i}Bu)$_3$] on meso H-ZSM-5-$_{250}$: (Si/Al = 25) in magenta, (Si/Al = 50) in brown, (Si/Al = 100) in red, (Si/Al = 200) in blue and (Si/Al = ∞) in black. Right: Selectivity in wt% of aromatics (full) of Ga(^{i}Bu)$_3$/meso H-ZSM-5-$_{250}$ Conditions: T = 580 °C, total flow = 10 mL.min^{-1} (5% of C3 in Ar). (For interpretation of the references to colour in this figure legend, the reader is referred to the web version of this article.)

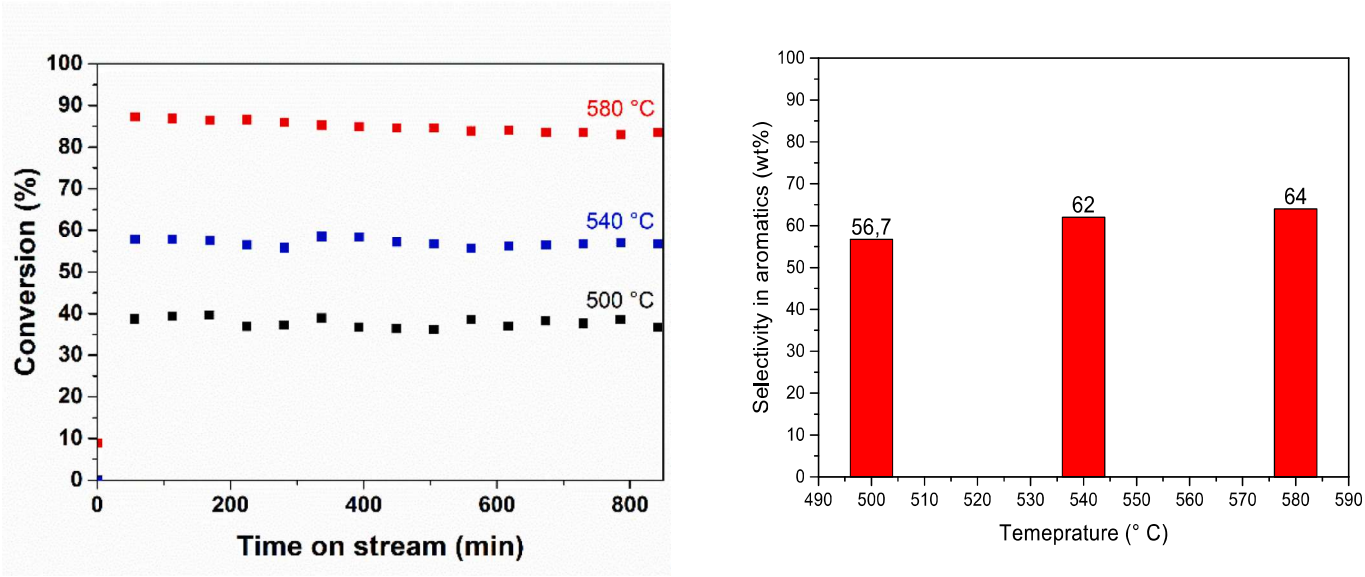

Fig. 7. Propane conversion (left) and selectivity in aromatics (right, in wt%) of Ga(^{i}Bu)$_3$/meso H-ZSM-5-$_{250}$ (Si/Al = 50) (B); Conditions: black curve at T = 500 °C, blue curve at T = 540 °C and red curve at T = 580 °C with a total flow = 10 mL.min^{-1} (5% of C3 in Ar). (For interpretation of the references to colour in this figure legend, the reader is referred to the web version of this article.)

to 500 °C led to the lowest conversion (Fig. 7, black curve) and selectivity toward aromatics among the three temperatures. Propane conversion decreased to 38% but seemed to be more stable over the time compared to the conversion at 580 °C, while the selectivity toward aromatics decreased slightly from 64 wt% to 56.7 wt%. At 540 °C, the C3 conversion was about 57% (Fig. 7, blue curve) with high stability as a function of time on stream and high selectivity toward aromatics with 62 wt%. The variation of the temperature from 500 to 580 °C showed that the best compromise between activity and selectivity to aromatics (high activity, 88% and selectivity toward BTX, 64 wt%) was obtained at 580 °C. Therefore, this temperature was selected to investigate the influence of the gas composition on the conversion and selectivity of Ga (iBu)$_3$/meso H-ZSM-5-$_{250}$ (Si/Al = 50) in propane aromatization.

When propane concentration in the feed was increased from 5 to 10%, the conversion decreased from 88% to around 72% (Fig. A24). The selectivity toward aromatics decreased as well from 64 wt% to 58 wt%. Increasing the propane concentration to 20% in Ar, the conversion reached its lowest (58%) and the selectivity toward aromatics decreased to 51.4 wt%.

To sum up, optimizing thermodynamic and kinetic parameters such as temperature and propane concentration in the feed shows that the most promising results were obtained at 580 °C with 5% of propane in the feed.

4. Conclusion

The main objective of this work is to investigate the effect of the Brønsted acidity over gallium immobilized H-ZSM-5 for propane aromatization and to determine the most promising reaction conditions. The first stage involves preparation of a series of H-ZSM-5 with different Si/Al ratio (Si/Al = 25, 50, 100, 200 and ∞) tuned by controlled addition of $NaAlO_2$ on fumed silica followed by desilication-delaumination to create the *meso*-pores. These materials were characterized by XRD, N_2 adsorption/desorption and EDX and served as support for gallium immobilization. Prior to grafting of the gallium precursor on the support, these materials were dehydroxylated at 250 °C and characterized by DRIFT, solid-state ^{1}H MAS NMR and N_2 adsorption/desorption. The grafting of [Ga(iBu)$_3$] occurred on the silanol sites of these *meso* H-ZSM-5-$_{250}$ (with Si/Al = 25, 50, 100, 200 and ∞) and led to a monopodal gallium species [(≡SiO)Ga(iBu)$_2$], evidenced by DRIFT, high field solid-state NMR (^{1}H and ^{13}C), N_2 adsorption/desorption, EXAFS as well as mass balance analysis. Importantly, the immobilization of Ga occurred selectively on the silanol groups located in the *meso*pores while the Brønsted acid site located in the micro pores remained intact due to judicious choice of the organometallic precursor having a particular kinetic diameter to only enter the meso pores. Thus, bifunctional catalysts including Ga sites for dehydrogenation and Brønsted acid sites for aromatization were obtained and they were tested in propane aromatization. The gallium functionalized materials exhibited higher activity and selectivity compared to the pristine zeolites support which gave mainly propane cracking products. This result confirmed the role of Ga and its high capacity of dehydrogenating propane into propene. The effect of Si/Al ratio on the catalytic performance of the catalyst as well as the distribution in the reaction products were evaluated. At low Si/Al ratio of meso H-ZSM-5-$_{250}$ (25 and 50), a very high activity and selectivity toward the aromatics was obtained compared to Ga(iBu)$_3$/meso H-ZSM-5-$_{250}$ (Si/Al = 100 and 200). Simultaneously, the lack of acidity in high ratios of Si/Al led to a low formation of aromatics compounds. On non-acidic meso H-ZSM-5-$_{250}$ (Si/Al = ∞), aromatic compounds were absent, and a very low activity was obtained. Operating at lower temperature results in a considerably lower conversion and selectivity toward aromatics. The variation of the gas composition in the feed affected the activity and the selectivity of products; the most promising results were obtained at lower concentration of propane in the feed. Supplementary studies and characterization techniques are required to further investigate the Ga species formed under the operating conditions, as well as their potential role in catalysis.

CRediT authorship contribution statement

Abou Nakad Jessy: Methodology, Writing – original draft, Investigation. **Daniel Firth:** Investigation, Methodology, Writing – original draft. **Muhammad Taoheed Bisiriyu:** Investigation, Validation. **Kai C. Szeto:** Supervision, Writing – original draft, Writing – review & editing. **Nicolas Merle:** Investigation, Writing – original draft. **Aimery De Mallmann:** Formal analysis, Investigation, Writing – original draft – review & editing. **Régis M. Gauvin:** Methodology, Writing – original draft. **Laurent Delevoye:** Investigation, Validation, Writing – original draft. **Unni Olsbye:** Methodology, Supervision, Writing – original draft. **Mostafa Taoufik:** Conceptualization, Methodology, Project

administration, Supervision, Writing – original draft, Writing – review & editing.

Declaration of Competing Interest

The authors declare that they have no known competing financial interests or personal relationships that could have appeared to influence the work reported in this paper.

Jessy ABOU NAKAD reports financial support was provided by E. U. H2020 BIZEOLCAT Project. Daniel FIRTH reports financial support was provided by E. U. H2020 BIZEOLCAT Project.

Data availability

Data will be made available on request.

Acknowledgments

This work was carried out as a part of BIZEOLCAT project, which has received funding from the European Union's Horizon 2020 research and innovation program under grant agreement No. 814671. In particular, J. A. is grateful for her PhD grant. AdM thanks Olivier Mathon and Kiril Lomachenko for their help during the recording of the X-ray absorption spectra at ESRF, on beam line BM23.

Appendix A. Supplementary data

Supplementary data to this article can be found online at https://doi.org/10.1016/j.catcom.2023.106825.

References

[1] Z. Chen, E. Rodriguez, R. Agrawal, Toward carbon neutrality for natural gas liquids valorization fromShale gas, Ind. Eng. Chem. Res. 61 (2022) 4469–4474, https://doi.org/10.1021/acs.iecr.1c04913.
[2] S. Hajimirzaee, A. Soleimani Mehr, E. Kianfar, Modified ZSM-5 zeolite for conversion of LPG to aromatics, Polycycl. Aromat. Compd. 42 (2022) 2334–2347, https://doi.org/10.1080/10406638.2020.1833048.
[3] K. Wang, M. Dong, J. Li, P. Liu, K. Zhang, J. Wang, W. Fan, Facile fabrication of ZSM-5 zeolite hollow spheres for catalytic conversion of methanol to aromatics, Catal. Sci. Technol. 7 (2017) 560–564, https://doi.org/10.1039/c6cy02476a.
[4] P. Zhang, L. Tan, G. Yang, N. Tsubaki, One-pass selective conversion of syngas to *Para*-xylene, Chem. Sci. 8 (2017) 7941–7946, https://doi.org/10.1039/c7sc03427j.
[5] J. Zhang, M. Zhang, S. Chen, X. Wang, Z. Zhou, Y. Wu, T. Zhang, G. Yang, Y. Han, Y. Tan, Hydrogenation of CO_2 into aromatics over a $ZnCrO_x$-zeolite composite catalyst, Chem. Commun. 55 (2019) 973–976, https://doi.org/10.1039/c8cc09019j.
[6] A. Bhan, W.N. Delgass, Propane aromatization over HZSM-5 and Ga/HZSM-5 catalysts, Catal. Rev.-Sci. Eng. 50 (2008) 19–151, https://doi.org/10.1080/01614940701804745.
[7] J.J. Spivey, G. Hutchings, Catalytic aromatization of methane, Chem. Soc. Rev. 43 (2014) 792–803, https://doi.org/10.1039/c3cs60259a.
[8] P. Schulz, M. Baerns, Aromatization of ethane over gallium-promoted H-ZSM-5 catalysts, Appl. Catal. 78 (1991) 15–29, https://doi.org/10.1016/0166-9834(91)80086-C.
[9] G. Price, V. Kanazirev, K. Dooley, V. Hart, On the mechanism of propane dehydrocyclization over cation-containing, proton-poor MFI zeolite, J. Catal. 173 (1998) 17–27, https://doi.org/10.1006/jcat.1997.1891.
[10] M. Raad, S. Hamieh, J. Toufaily, T. Hamieh, L. Pinard, Propane aromatization on hierarchical Ga/HZSM-5 catalysts, J. Catal. 366 (2018) 223–236, https://doi.org/10.1016/j.jcat.2018.07.035.
[11] M. Raad, A. Astafan, S. Hamieh, J. Toufaily, T. Hamieh, J.D. Comparot, C. Canaff, T.J. Daou, J. Patarin, L. Pinard, Catalytic properties of Ga-containing MFI-type zeolite in cyclohexane dehydrogenation and propane aromatization, J. Catal. 365 (2018) 376–390, https://doi.org/10.1016/j.jcat.2018.06.029.
[12] G. Caeiro, R.H. Carvalho, X. Wang, M.A.N.D.A. Lemos, F. Lemos, M. Guisnet, F. R. Ribeiro, Activation of C_2-C_4 alkanes over acid and bifunctional zeolite catalysts, J. Mol. Catal. A Chem. 255 (2006) 131–158, https://doi.org/10.1016/j.molcata.2006.03.068.
[13] M. Guisnet, N. Gnep, H. Vasques, F. Ribeiro, Zn-doped HZSM5 Catalysts for Propane Aromatization, in: P. Jacobs, N. Jaeger, L. Kubelkova, B. Wichterlova (Eds.), Stud. Surf. Sci. Catal., 1991, pp. 321–329.
[14] V. de O. Rodrigues, A.C. Faro Junior, On catalyst activation and reaction mechanisms in propane aromatization on Ga/HZSM5 catalysts, Appl. Catal. A Gen. 435 (2012) 68–77, https://doi.org/10.1016/j.apcata.2012.05.036.
[15] W. Zhou, J. Liu, J. Wang, L. Lin, X. Zhang, N. He, C. Liu, H. Guo, Enhancing propane aromatization performance of Zn/H-ZSM-5 zeolite catalyst with Pt promotion: effect of the third metal additive-Sn, Catal. Lett. 149 (2019) 2064–2077, https://doi.org/10.1007/s10562-019-02832-5.
[16] P. Meriaudeau, G. Sapaly, C. Naccache, Dual function mechanism of alkane aromatization over H-ZSM-5 supported Ga, Zn, Pt catalysts - respective role of acidity and additive, in: T. Inui, S. Namba, T. Tatsumi (Eds.), Stud. Surf. Sci. Catal., 1991, pp. 267–279.
[17] A. Samanta, X. Bai, B. Robinson, H. Chen, J. Hu, Conversion of light alkane to value-added chemicals over ZSM-5/metal promoted catalysts, Ind. Eng. Chem. Res. 56 (2017) 11006–11012, https://doi.org/10.1021/acs.iecr.7b02095.
[18] M. Guisnet, N. Gnep, F. Alario, Aromatization of short chain alkanes on zeolite catalysts, Appl. Catal. A Gen. 89 (1992) 1–30, https://doi.org/10.1016/0926-860X(92)80075-N.
[19] Y. Joshi, K. Thomson, The roles of gallium hydride and Bronsted acidity in light alkane dehydrogenation mechanisms using Ga-exchanged HZSM-5 catalysts: a DFT pathway analysis, Catal. Today 105 (2005) 106–121, https://doi.org/10.1016/j.cattod.2005.04.017.
[20] H. Xiao, J. Zhang, X. Wang, Q. Zhang, H. Xie, Y. Han, Y. Tan, A highly efficient Ga/ZSM-5 catalyst prepared by formic acid impregnation and *in situ* treatment for propane aromatization, Catal. Sci. Technol. 5 (2015) 4081–4090, https://doi.org/10.1039/c5cy00665a.
[21] G. Krishnamurthy, A. Bhan, W.N. Delgass, Identity and chemical function of gallium species inferred from microkinetic modeling studies of propane aromatization over Ga/HZSM-5 catalysts, J. Catal. 271 (2010) 370–385, https://doi.org/10.1016/j.jcat.2010.02.026.
[22] R. Mao, J. Yao, R. Carli, Gallium containing hybrid catalysts for the aromatization of Normal-butane, Appl. Catal. A Gen. 86 (1992) 127–138.
[23] K. Dooley, C. Chang, G. Price, Effects of pretreatments on state of gallium and aromatization activity of gallium ZSM-5 catalysts, Appl. Catal. A Gen. 84 (1992) 17–30, https://doi.org/10.1016/0926-860X(92)80336-B.
[24] V. Choudhary, K. Mantri, C. Sivadinarayana, Influence of zeolite factors affecting zeolitic acidity on the propane aromatization activity and selectivity of Ga/H-ZSM-5, Microporous Mesoporous Mater. 37 (2000) 1–8, https://doi.org/10.1016/S1387-1811(99)00185-7.
[25] G. Price, V. Kanazirev, Ga2O3/HZSM-5 propane aromatization catalysts - formation of active-centers via solid-state reaction, J. Catal. 126 (1990) 267–278, https://doi.org/10.1016/0021-9517(90)90065-R.
[26] B. Kwak, W. Sachtler, Effect of Ga/proton balance in Ga/HZSM-5 catalysts on C-3 conversion to aromatics, J. Catal. 145 (1994) 456–463, https://doi.org/10.1006/jcat.1994.1056.
[27] G. Meitzner, E. Iglesia, J. Baumgartner, E. Huang, The chemical-state of gallium in working alkane Dehydrocyclodimerization catalysts - Insitu gallium K-edge X-ray absorption-spectroscopy, J. Catal. 140 (1993) 209–225, https://doi.org/10.1006/jcat.1993.1079.
[28] E. El-Malki, R. van Santen, W. Sachtler, Introduction of Zn, Ga, and Fe into HZSM-5 cavities by sublimation: identification of acid sites, J. Phys. Chem. B 103 (1999) 4611–4622, https://doi.org/10.1021/jp990116l.
[29] P. Meriaudeau, C. Naccache, Gallium based MFI zeolites for the aromatization of propane, Catal. Today 31 (1996) 265–273, https://doi.org/10.1016/S0920-5861(96)00017-X.
[30] T.E. Tshabalala, M.S. Scurrell, Aromatization of *n*-hexane over Ga, Mo and Zn modified H-ZSM-5 zeolite catalysts, Catal. Commun. 72 (2015) 49–52, https://doi.org/10.1016/j.catcom.2015.06.022.
[31] M. Xin, E. Xing, X. Gao, Y. Wang, Y. Ouyang, G. Xu, Y. Luo, X. Shu, Ga substitution during modification of ZSM-5 and its influences on catalytic aromatization performance, Ind. Eng. Chem. Res. 58 (2019) 6970–6981, https://doi.org/10.1021/acs.iecr.9b00295.
[32] V. de O. Rodrigues, J.-G. Eon, A.C. Faro Jr., Correlations between dispersion, acidity, reducibility, and propane aromatization activity of gallium species supported on HZSM5 zeolites, J. Phys. Chem. C 114 (2010) 4557–4567, https://doi.org/10.1021/jp910642p.
[33] P. Gao, J. Xu, G. Qi, C. Wang, Q. Wang, Y. Zhao, Y. Zhang, N. Feng, X. Zhao, J. Li, F. Deng, A mechanistic study of methanol-to-aromatics reaction over Ga-modified ZSM-5 zeolites: understanding the dehydrogenation process, ACS Catal. 8 (2018) 9809–9820, https://doi.org/10.1021/acscatal.8b03076.
[34] V. Kazansky, I. Subbotina, R. van Santen, E. Hensen, DRIFTS study of the nature and chemical reactivity of gallium ions in Ga/ZSM-5 II. Oxidation of reduced Ga species in ZSM-5 by nitrous oxide or water, J. Catal. 233 (2005) 351–358, https://doi.org/10.1016/j.jcat.2005.05.004.
[35] E. Hensen, M. García-Sánchez, N. Rane, P. Magusin, P. Liu, K. Chao, R. van Santen, *In situ* GaK edge XANES study of the activation of Ga/ZSM-5 prepared by chemical vapor deposition of trimethylgallium, Catal. Lett. 101 (2005) 79–85, https://doi.org/10.1007/s10562-004-3753-x.
[36] S.D. Fleischman, S.L. Scott, Evidence for the pairwise disposition of grafting sites on highly Dehydroxylated Silicas via their reactions with $Ga(CH_3)_3$, J. Am. Chem. Soc. 133 (2011) 4847–4855, https://doi.org/10.1021/ja108905p.
[37] Z. Taha, E. Deguns, S. Chattopadhyay, S. Scott, Formation of digallium sites in the reaction of trimethylgallium with silica, Organometallics 25 (2006) 1891–1899, https://doi.org/10.1021/om051034o.
[38] K.C. Szeto, A. Gallo, S. Hernandez-Morejudo, U. Olsbye, A. De Mallmann, F. Lefebvre, R.M. Gauvin, L. Deevoye, S.L. Scott, M. Taoufik, Selective grafting of Ga(i-Bu)(3) on the Silanols of mesoporous H-ZSM-5 by surface organometallic chemistry, J. Phys. Chem. C 119 (2015) 26611–26619, https://doi.org/10.1021/acs.jpcc.5b09289.

[39] R. Kovar, H. Derr, D. Brandau, J. Callaway, Preparation of Organogallium compounds from Organolithium reagents and gallium chloride - infrared, magnetic-resonance, and mass-spectral studies of Alkylgallium compounds, Inorg. Chem. 14 (1975) 2809–2814, https://doi.org/10.1021/ic50153a042.

[40] P. Jacobs, J.A. Martens, Chapter I: Synthesis of ZSM-5 Zeolites in the Presence of Tetrapropylammonium Ions, Elsevier, 1987, pp. 47–111.

[41] H.M. Sun, P. Peng, Y.H. Wang, C.C. Li, F. Subhan, W. Xing, Z.D. Zhang, Z.Y. Liu, Z. F. Yan, Preparation, scale-up and application of meso-ZSM-5 zeolite by sequential desilication-dealumination, J. Porous. Mater. 24 (2017) 1513–1525, https://doi.org/10.1007/s10934-017-0391-4.

[42] O. Mathon, A. Beteva, J. Borrel, D. Bugnazet, S. Gatla, R. Hino, I. Kantor, T. Mairs, M. Munoz, S. Pasternak, F. Perrin, S. Pascarelli, The time-resolved and extreme conditions XAS (TEXAS) facility at the European Synchrotron Radiation Facility: the general-purpose EXAFS bending-magnet beamline BM23, J. Synchrotron Radiat. 22 (2015) 1548–1554, https://doi.org/10.1107/S1600577515017786.

[43] B. Ravel, M. Newville, ATHENA, ARTEMIS, HEPHAESTUS: data analysis for X-ray absorption spectroscopy using IFEFFIT, J. Synchrotron Radiat. 12 (2005) 537–541, https://doi.org/10.1107/S0909049505012719.

[44] A. Michalowicz, J. Moscovici, D. Muller-Bouvet, K. Provost, MAX: Multiplatform Applications for XAFS, A. DiCicco, A. Filipponi (Eds.), J. Phys. Conf. Ser. 190 (2009) 012034. doi:https://doi.org/10.1088/1742-6596/190/1/012034.

[45] A. Ankudinov, B. Ravel, J. Rehr, S. Conradson, Real-space multiple-scattering calculation and interpretation of x-ray-absorption near-edge structure, Phys. Rev. B 58 (1998) 7565–7576, https://doi.org/10.1103/PhysRevB.58.7565.

[46] S.M. Auerbach, K.A. Carrado, P.K. Dutta, Handbook of Zeolite Science and Technology, CRC Press, 2003, https://doi.org/10.1201/9780203911167.

[47] M. Davis, Ordered porous materials for emerging applications, Nature 417 (2002) 813–821, https://doi.org/10.1038/nature00785.

[48] A. Corma, State of the art and future challenges of zeolites as catalysts, J. Catal. 216 (2003) 298–312, https://doi.org/10.1016/S0021-9517(02)00132-X.

[49] T. He, Y. Wang, P. Miao, J. Li, J. Wu, Y. Fang, Hydrogenation of naphthalene over noble metal supported on mesoporous zeolite in the absence and presence of sulfur, Fuel 106 (2013) 365–371, https://doi.org/10.1016/j.fuel.2012.12.025.

[50] Y. Wang, T. He, K. Liu, J. Wu, Y. Fang, From biomass to advanced bio-fuel by catalytic pyrolysis/hydro-processing: Hydrodeoxygenation of bio-oil derived from biomass catalytic pyrolysis, Bioresour. Technol. 108 (2012) 280–284, https://doi.org/10.1016/j.biortech.2011.12.132.

[51] Y. Wang, Y. Fang, T. He, H. Hu, J. Wu, Hydrodeoxygenation of dibenzofuran over noble metal supported on mesoporous zeolite, Catal. Commun. 12 (2011) 1201–1205, https://doi.org/10.1016/j.catcom.2011.04.010.

[52] S. van Donk, A. Janssen, J. Bitter, K. de Jong, Generation, characterization, and impact of mesopores in zeolite catalysts, Catal. Rev.-Sci. Eng. 45 (2003) 297–319, https://doi.org/10.1081/CR-120023908.

[53] T. Tsai, S. Liu, I. Wang, Disproportionation and transalkylation of alkylbenzenes over zeolite catalysts, Appl. Catal. A Gen. 181 (1999) 355–398, https://doi.org/10.1016/S0926-860X(98)00396-2.

[54] Y. Ji, H. Yang, W. Yan, Strategies to enhance the catalytic performance of ZSM-5 zeolite in hydrocarbon cracking: a review, Catalysts 7 (2017) 367, https://doi.org/10.3390/catal7120367.

[55] L. Xue, K. Cheng, H. Zhang, W. Deng, Q. Zhang, Y. Wang, Mesoporous H-ZSM-5 as an efficient catalyst for conversions of cellulose and cellobiose into methyl glucosides in methanol, Catal. Today 274 (2016) 60–66, https://doi.org/10.1016/j.cattod.2016.01.055.

[56] L. Shirazi, E. Jamshidi, M.R. Ghasemi, The effect of Si/Al ratio of ZSM-5 zeolite on its morphology, acidity and crystal size, Cryst. Res. Technol. 43 (2008) 1300–1306, https://doi.org/10.1002/crat.200800149.

[57] Y. Bouhoute, D. Grekov, K.C. Szeto, N. Merle, A. De Mallmann, F. Lefebvre, G. Raffa, I. Del Rosal, L. Maron, R.M. Gauvin, L. Delevoye, M. Taoufik, Accessing realistic models for the WO3-SiO2 industrial catalyst through the Design of Organometallic Precursors, ACS Catal. 6 (2016) 1–18, https://doi.org/10.1021/acscatal.5b01744.

[58] V. Riollet, M. Taoufik, J.-M. Basset, F. Lefebvre, Reactivity of silica-supported zirconium neopentyl fragments with trimethylphosphine and acetone: formation of unexpected reaction products, J. Organomet. Chem. 692 (2007) 4193–4195, https://doi.org/10.1016/j.jorganchem.2007.06.038.

[59] K.D.M. Harris, M. Xu, J.M. Thomas, Probing the evolution of water clusters during hydration of the solid acid catalyst H-ZSM-5, Philos. Mag. 89 (2009) 3001–3012, https://doi.org/10.1080/14786430903164606.

[60] E. Brunner, H. Ernst, D. Freude, M. Hunger, C.B. Krause, D. Prager, W. Reschetilowski, W. Schwieger, K.-H. Bergk, Solid-state NMR and catalytic studies of mildly hydrothermally dealuminated HZSM-5, Zeolites 9 (1989) 282–286, https://doi.org/10.1016/0144-2449(89)90072-9.

[61] H. Huo, L. Peng, C.P. Grey, Low temperature 1H MAS NMR spectroscopy studies of proton motion in zeolite HZSM-5, J. Phys. Chem. C 113 (2009) 8211–8219, https://doi.org/10.1021/jp900313y.

[62] K. Chen, M. Abdolrhamani, E. Sheets, J. Freeman, G. Ward, J.L. White, Direct detection of multiple acidic proton sites in zeolite HZSM-5, J. Am. Chem. Soc. 139 (2017) 18698–18704, https://doi.org/10.1021/jacs.7b10940.

[63] F. Deng, Y. Yue, C. Ye, 1H/27Al TRAPDOR NMR studies on aluminum species in dealuminated zeolites, Solid State Nucl. Magn. Reson. 10 (1998) 151–160, https://doi.org/10.1016/S0926-2040(97)00028-3.

[64] L. Beck, J. Haw, Multinuclear NMR-studies reveal a complex acid function for zeolite-beta, J. Phys. Chem. 99 (1995) 1076–1079, https://doi.org/10.1021/j100004a004.

[65] M. Hunger, Bronsted acid sites in zeolites characterized by multinuclear solid-state NMR spectroscopy, Catal. Rev.-Sci. Eng. 39 (1997) 345–393, https://doi.org/10.1080/01614949708007100.

[66] E.J.M. Hensen, D.G. Poduval, V. Degirmenci, D.A.J.M. Ligthart, W. Chen, F. Mauge, M.S. Rigutto, J.A.R. van Veen, Acidity characterization of amorphous silica-alumina, J. Phys. Chem. C 116 (2012) 21416–21429, https://doi.org/10.1021/jp309182f.

[67] J. Lercher, R. van Santen, H. Vinek, Carbonium-ion formation in zeolite catalysis, Catal. Lett. 27 (1994) 91–96, https://doi.org/10.1007/BF00806981.

[68] G. Piccini, M. Alessio, J. Sauer, Y. Zhi, Y. Liu, R. Kolvenbach, A. Jentys, J. A. Lercher, Accurate adsorption thermodynamics of small alkanes in zeolites. Ab initio theory and experiment for H-Chabazite, J. Phys. Chem. C. 119 (2015) 6128–6137, https://doi.org/10.1021/acs.jpcc.5b01739.

[69] W. Uhl, L. Cuypers, G. Geiseler, K. Harms, W. Massa, Syntheses and crystal structures of dialkylgallium hydrides - dimeric versus trimeric formula units, Z. Anorg. Allg. Chem. 628 (2002) 1001–1006, https://doi.org/10.1002/1521-3749(200206)628:5<1001::AID-ZAAC1001>3.0.CO;2-N.

[70] R. Duchateau, T. Dijkstra, R. van Santen, G. Yap, Silsesquioxane models for silica surface silanol sites with adjacent siloxide functionalites and olefin polymerization catalysts thereof, Chem. Eur. J. 10 (2004) 3979–3990, https://doi.org/10.1002/chem.200400206.

[71] S. Basharat, W. Betchley, C.J. Carmalt, S. Barnett, D.A. Tocher, H.O. Davies, Synthesis of group 13 sesquialkoxides and their application as precursors to crystalline oxide films, Organometallics 26 (2007) 403–407, https://doi.org/10.1021/om0608657.

[72] B. Xu, M. Tan, X. Wu, H. Geng, F. Song, Q. Ma, C. Luan, G. Yang, Y. Tan, Effects of silylation on Ga/HZSM-5 for improved propane dehydroaromatization, Fuel 283 (2021), https://doi.org/10.1016/j.fuel.2020.118889.

[73] J.J.H.B. Sattler, J. Ruiz-Martinez, E. Santillan-Jimenez, B.M. Weckhuysen, Catalytic dehydrogenation of light alkanes on metals and metal oxides, Chem. Rev. 114 (2014) 10613–10653, https://doi.org/10.1021/cr5002436.

[74] V. Choudhary, P. Devadas, Product selectivity and aromatics distribution in aromatization of propane over H-GaMFI zeolite: influence of temperature, Microporous Mesoporous Mater. 23 (1998) 231–238, https://doi.org/10.1016/S1387-1811(98)00112-7.

[75] T. Choudhary, A. Kinage, S. Banerjee, V. Choudhary, Effect of temperature on the product selectivity and aromatics distribution in aromatization of propane over H-GaAlMFI zeolite, Microporous Mesoporous Mater. 70 (2004) 37–42, https://doi.org/10.1016/j.micromeso.2004.01.010.